Interface Unbinding in Structured Wedges

Gilberto Giugliarelli

Dipartimento di Fisica, Università di Udine, I–33100 Udine, Italy and
INFM–Dipartimento di Fisica, Università di Padova, I–35131 Padova, Italy

The unbinding properties of an interface near structured wedges are investigated by discrete models with short range interactions. The calculations demonstrate that interface unbinding take place in two stages: *i*) a continuous filling–like transition in the pure wedge–like parts of the structure; *ii*) a conclusive discontinuous unbinding. In $2D$ an exact transfer matrix approach allows to extract the whole interface phase diagram and the precise mechanism at the basis of the phenomenon. The Metropolis Monte Carlo simulations performed in $3D$ reveal an analogous behavior. The emerging scenario allows to shed new light onto the problem of wetting of geometrically rough walls.

I. INTRODUCTION

Wetting phenomena concerns the properties of the liquid film which forms when an undersaturated vapor (fluid) is put in contact with a solid inert substrate. The critical properties of the liquid–vapor interface are, generally, determined by nature and range of the intervening interactions. In this respect, e.g. for a planar substrate, different interactions potentials determine the applicability of partial or complete wetting regimes as well as the nature of the wetting transition (for a review on these phenomena see [1, 2]).

However, substrate surface geometry can strongly influence these properties. For example, in the complete wetting regime, adsorption isotherms of random rough substrates [3, 4] and linearly sculpted substrates [5, 6, 7] exhibit unusual exponents which are determined by the surface geometry. On the other hand, while for planar geometry partial wetting prevents the growth of macroscopic films, in the same conditions, in pure wedges, we can have continuous filling phenomena by which the film thickness is driven to infinity [5, 8]. Finally, and this is particularly relevant for wetting critical properties, there are many indications that increasing surface roughness can change the order of the wetting transition to first–order [9, 10, 11, 12].

In this paper we report the results of an accurate investigation about the unbinding properties of a thermally fluctuating interface in wedge–modified systems (see Fig. 1), we denoted *structured wedges* (SW). The choice of such a system structure is motivated by the fact that they incorporate contrasting geometrical motives (like wedges and ridges) which are typical of the geometry of rough surfaces. In this respect, while the separate effects of these geometries on wetting phenomena are already rather well known [8, 13], the effects of their combination were never approached in detail before. Here, we consider the study of both $2D$ (Fig. 1(a)) and $3D$ (Fig. 1(b)) SWs, and our results show that such structures implies two stage interface unbinding transition, one of which discontinuous. Our analysis of the phenomenon allows to understand its intimate connection with the surface geometry as well as to make some extension to the wetting properties of rough boundaries.

II. THE MODEL

In the framework of solid on solid (SOS) approach our model liquid–vapor interface corresponds to a lattice random walk (in $2D$) or to a random surface (in $3D$) in the vicinity of a fixed substrate boundary. If H_X denotes the substrate boundary (integer) height at the position X (depending on $2D$ or $3D$ space dimension, X denotes a single variable x or a couple of variable (x, y), respectively), the interface configurations can be specified in terms of the local relative (integer) height variables z_X (see Fig. 2). The discrete nature of the model, implies that non horizontal walls (see the magnifying glass in Fig. 1) are shaped as staircases with slopes not exceeding unity. Consequently, the height function H_X satisfy the conditions $H_{x+1} - H_x = 0, \pm 1$ and $H_{x+1,y} - H_{x,y} = 0, \pm 1$ in $2D$ and $3D$, respectively. In $3D$, because of the translation invariance along y axis, one has also $H_{x,y+1} - H_{x,y} = 0$.
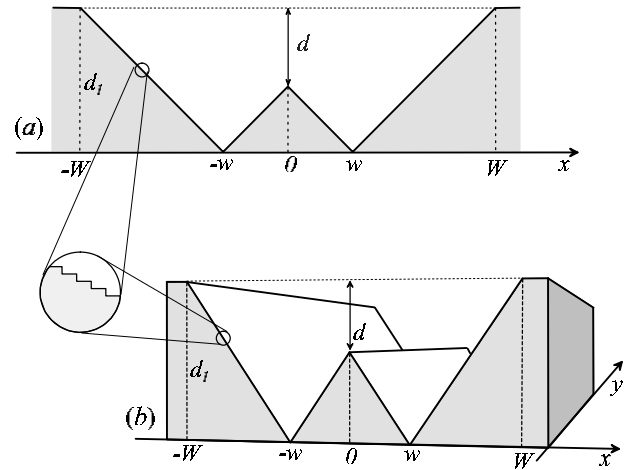

FIG. 1. Sketch of the $2D$ (panel (a)) and $3D$ (panel (b)) SW geometries studied in this paper. The *magnifying glass* shows the staircase nature of the tilted smooth walls (with slope $|1/n|$) by which the SW are constructed.

At coexistence (no chemical potential differences with respect to its critical bulk value), an interface (see Fig. 2(a), (b)), can be studied in terms of an Hamiltonian of

the form

$$\mathcal{H} = \sum_{\langle X,X'\rangle} \mathcal{E}(1 + |h_X - h_{X'}|^\gamma) - \mathcal{U}\sum_{X} \delta_{z_X,0}, \quad (1)$$

where the first sum is done over all pairs of nearest neighbor columns. In the above expression $\mathcal{E}$ and $-\mathcal{U}$ (with $\mathcal{E},\mathcal{U} > 0$) are the energy cost of any interface step (or plaquette in $3D$) and the energy gain of each interface contact (of horizontal step or plaquette) with the substrate, respectively; $\gamma = 1$ or ∞ determines the SOS or restricted SOS (RSOS) character of the implemented walk model, respectively. To limit the computational complexity, in $3D$ we consider only RSOS interfaces.
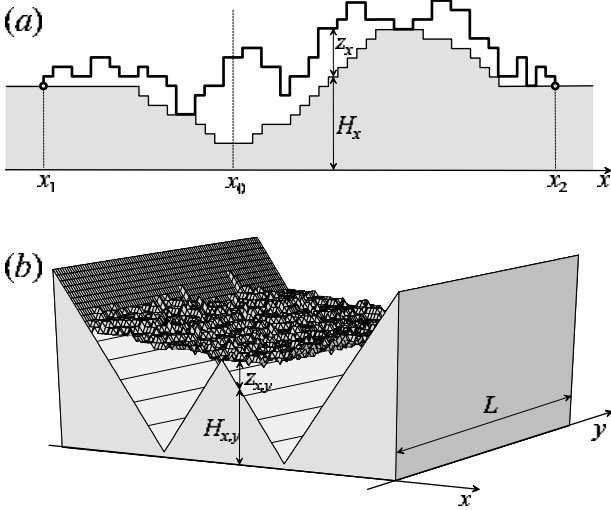

FIG. 2. (a) Example of a configuration of a directed walk (heavy continuous line) with the ends anchored to a $2D$ boundary (light continuous line delimiting the shaded area). (b) An RSOS interface–surface configuration near our $3D$ SW.

III. $2D$ STRUCTURED WEDGES

In $2D$, an interface in the vicinity of a boundary (with a generic shape) can be fully treated by a transfer matrix approach based on the matrices $\hat{R}_x$ and $\hat{L}_x$ defined as follows

$$[\hat{R}_x]_{z,z'} = \omega^{|z'-z+H_{x+1}-H_x|^\gamma} k^{\delta_{z',0}}, \quad (2a)$$

$$[\hat{L}_x]_{z,z'} = \omega^{|z'-z+H_{x-1}-H_x|^\gamma} k^{\delta_{z',0}}. \quad (2b)$$

Here $\omega = e^{-\mathcal{E}/k_BT} = e^{-1/t}$ ($t = k_BT/\mathcal{E}$) and $k = e^{U/k_BT} = e^{u/t}$ ($u = U/\mathcal{E}$) correspond to step and wall fugacities and, by definition, $\omega[R_x]_{z,z'}$ and $\omega[L_x]_{z,z'}$ are the Boltzmann weights of the elementary walks from $(x, H_x + z)$ to $(x + 1, H_{x+1} + z')$ or $(x - 1, H_{x-1} + z')$, respectively. Thus, the partition function of, e.g. the walks between (x_1, H_{x_1}) and (x_2, H_{x_2}) (see Fig. 2(a)), is given by

$$\mathcal{Z}_{x_1,x_2} = \omega^{x_2-x_1}[\hat{R}_{x_1\to x_2}]_{0,0} \equiv \omega^{x_2-x_1}[\hat{L}_{x_1\leftarrow x_2}]_{0,0}, \quad (3)$$

with $\hat{R}_{x\to x'} \equiv \prod_{i=x}^{x'-1} \hat{R}_i$ and $\hat{L}_{x\leftarrow x'} \equiv \prod_{i=x'}^{x+1} \hat{L}_i$

But the transfer matrix approach allows also the direct calculation of the distance probability distribution function (PDF) at any position along the boundary. A walk like the one in Fig. 2(a) can be divided in two parts, e.g. at x_0, obtaining two walks with Boltzmann weights $[\hat{R}_{x_1\to x_0}]_{0,z}$ and $[\hat{L}_{x_0\leftarrow x_2}]_{0,z}$, respectively. Thus, the walk distance PDF at x_0 is proportional to the product $[\hat{R}_{x_1\to x_0}]_{0,z} \cdot [\hat{L}_{x_0\leftarrow x_2}]_{0,z}$. On the other hand, *storing* the initial walk distance distributions, at x_1 and x_2, in the vectors r_{x_1} and l_{x_2} (in the case of Fig. 2(a) we should set $[r_{x_1}]_z = [l_{x_2}]_z = \delta_{z,0}$), the following iterations

$$r_{x+1} = r_x\hat{R}_x; \qquad l_{x-1} = l_x\hat{L}_x, \quad (4)$$

allows to get the quantities $[\hat{R}_{x_1\to x_0}]_{0,z}$ and $[\hat{L}_{x_0\leftarrow x_2}]_{0,z}$ in terms of the components of r_{x_0} and l_{x_0} vectors. Indeed, iterations (4) transfer toward right and left the local walk distance distributions to any position along the boundary, like in a forward diffusion process. Therefore, in the limit of an indefinite walk (our interface model), i.e. $|x_0 - x_{1,2}| \to \infty$, the transferred right and left PDFs, defined as

$$P_{x_0}^{(R)}(z) = \frac{1}{[r_{x_0}]}[r_{x_0}]_z; \qquad P_{x_0}^{(L)}(z) = \frac{1}{[l_{x_0}]}[l_{x_0}]_z, \quad (5)$$

will reach steady profiles depending only on the specific boundary conformation. In these conditions the interface PDF at any position x_0 will be given by

$$P_{x_0}(z) = P_{x_0}^{(R)}(z)P_{x_0}^{(L)}(z), \quad (6)$$

and the quantity

$$\Delta f_{x_0} = -\ln P_{x_0}(z) = -\left[\ln P_{x_0}^{(R)}(z) + \ln P_{x_0}^{(L)}(z)\right], \quad (7)$$

can be seen as the corresponding local excess interface free energy profile.

Our SWs boundaries contain only unit vertical steps. Thus, the transfer matrices (2) can be of only three different forms, i.e. those corresponding to a down step, an up step and no vertical step; we denote these matrices as $\hat{D}$, $\hat{U}$ and $\hat{F}$, respectively. For tilted wall regions with slope $|1/n|$, the calculation of right and left PDFs can be done by implementing iterations (4) in terms of $\hat{F}^{n-1}\hat{D}$ or $\hat{F}^{n-1}\hat{U}$ matrices (depending on the descending or ascending character of the wall); for large system sizes, the corresponding $P^{(R)}$ and $P^{(L)}$ will asymptotically become eigenvectors of these matrices. In particular, in binding conditions (i.e. at high enough u values), the interface PDFs at $x = \pm w$ and $x = 0$ (see Fig. 1(a)) will correspond to Φ_n^2 and Ψ_n^2, Φ_n and Ψ_n being the bound eigenvectors of matrices $\hat{F}^{n-1}\hat{D}$ and $\hat{F}^{n-1}\hat{U}$, respectively. In this respect, an accurate investigation allows the determination of these states (exact for $n = 1, 2$, numerical for $n > 2$) both for SOS as well as RSOS walk models.

A brief analysis of $n = 1$ case (tilted walls with unit slope) is particularly useful for the understanding of the

general scenario. Matrices $\hat{\boldsymbol{F}}^{n-1}\hat{\boldsymbol{D}}$ and $\hat{\boldsymbol{F}}^{n-1}\hat{\boldsymbol{U}}$ reduce to $\hat{\boldsymbol{D}}$ and $\hat{\boldsymbol{U}}$ and for SOS walks both $\boldsymbol{\Phi}_1$ and $\boldsymbol{\Psi}_1$ components scale as $\mu_{D_1}^z$ and $\mu_{U_1}^z$, respectively. $\mu_{D_1} = \frac{1+k\omega^2}{k\omega}$, and thus the local character of $\boldsymbol{\Phi}_1$ (i.e. $\mu_{D_1} < 1$) is achieved until $k > k_{D_1,c}$, with $k_{D_1,c} = \frac{1}{\omega(1-\omega)}$. The corresponding interface PDF at the SW bottoms (i.e. $x = \pm w$) is $P_{\pm w}(z) = \mu_{D_1}^{2z}$ and the resulting interface average distance, $\langle z \rangle_{\pm w} = \frac{\sum_z z \cdot P_{\pm w}(z)}{\sum_z P_{\pm w}(z)}$ is given by

$$\langle z \rangle_{\pm w} = \frac{k}{(2 - k + k\omega^2)(1 + 2k\omega^2 + k^2\omega^4 - k^2\omega^2)}. \quad (8)$$

As $k \to k_{D_1,c}^+$, $\langle z \rangle_{\pm w}$ diverges with continuity as $[k - k_{D_1,c}]^{-1}$ and thus $k_{D_1,c}$ is the critical fugacity associated to the continuous interface unbinding from SW bottoms. This transition is the analog of the critical filling transition in pure wedge geometry [5, 14]. We have verified that for $n = 2, 3, \ldots, 10$ one observe the same behavior (also for RSOS walk model) and in Fig. 3 we show the corresponding phase–line boundaries, consisting in the the plot of the quantity $u_c(t) = t \ln k_{D_n,c}$. The picture demonstrate that in the wedge geometry, in contrast to the case of flat substrates (see the bottom curves in Fig. 3), a bound interface always (also at low t) requires a finite attraction energy u. On the other hand, the local minima in the phase–line boundaries confirm the possibility of reentrance phenomena which were already predicted [10] for rough self–affine boundaries. More details about these aspects will be reported elsewhere [15].
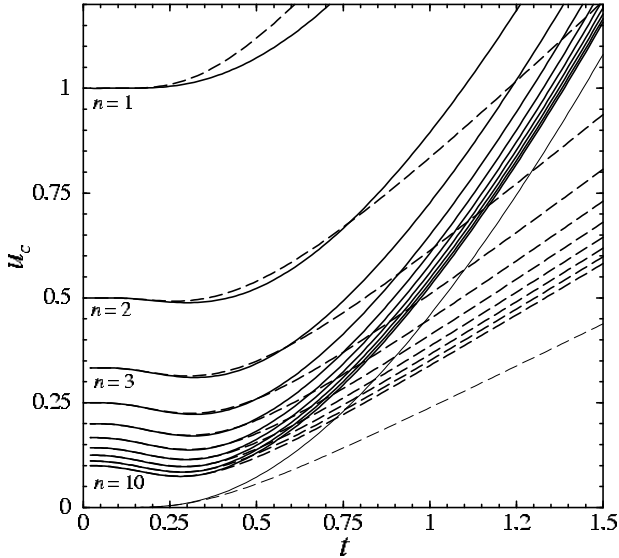

FIG. 3. SOS (continuous lines) and RSOS (dashed lines) interface phase–line boundaries in the u–t plane for $2D$ SWs (like in Fig. 1(a)) with tilted wall slope $|1/n|$ ($n = 1, 2, \ldots, 10$). Upper curves ($n = 1, 2$) are the result of exact calculations; the other curves were obtained by a numerical implementation of iterations (4). Lower (light) curves are the interface phase–line boundary for a flat wall [16].

On the contrary, $\mu_{U_1} = \frac{k\omega}{k-1}$ and therefore the local character of $\boldsymbol{\Psi}_1$ is achieved for $k > k_{U_1,c}$ with

$k_{U_1,c} = 1/(1 - \omega) < k_{D_1,c}$. Thus, when k approaches $k_{D_1,c}$ from above, and the interface unbinds from SW bottoms, it remains tightly bound to the central ridge. To be more precise, in the limit $k \to [k_{D_1,c}]^+$ the mean interface distance from the SW central ridge is finite and is given by

$$\langle z \rangle_0 = \frac{\omega^4(1 - \omega + \omega^2)}{(1 + \omega + \omega^2)(1 + \omega^2)(1 - \omega)^2}. \quad (9)$$

Finally, for $k < k_{D_1,c}$ we are out of binding conditions for $\hat{\boldsymbol{D}}$ matrix and the lateral descending walls of the SW are no more able to bind the walks: iterations (4), asymptotically produce delocalized right and left PDFs. In these conditions, the presence of the central ridge can have only very marginal effects (vanishing with the size of the structure) and, thus, the interface unbinds from the SW. The conclusion is: $k_{D_1,c}$ is also the threshold of a discontinuous unbinding transition! The curves in Fig. 3 can be seen also as the interface phase–lines for $2D$ SW first–order unbinding.
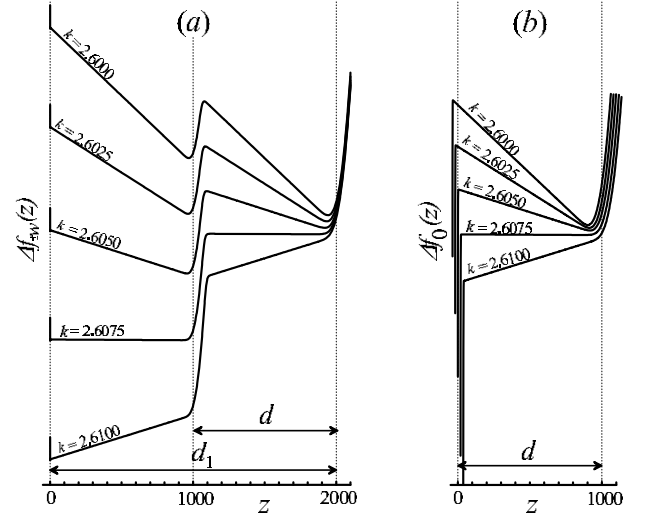

FIG. 4. Excess free energy profiles (in arbitrary units) at $x = \pm w$ (panel (a)) and $x = 0$ (panel (b)) for a $2D$ SW with wall slope $|1/2|$, $d = 1000$ and $d_1 = 2000$ (see Fig. 1(a)). The free energy profiles have been obtained by a numerical implementation of iterations (4) at $\omega = 0.2$ ($t = 0.6213\ldots$). The curves are shifted vertically to increase the picture clearness; in panel (b) also a little horizontal shift has been adopted to avoid curves superposition at $z = 0$.

The conclusive validation of the above, surprising, conclusion is obtained by the analysis of the free energy profiles. In Fig. 4 we show a plot of $\Delta f_{\pm w}(z)$ (panel (a)) and $\Delta f_0(z)$ (panel (b)) profiles obtained at fixed t for an RSOS interface in a finite size SW with wall slope $1/2$ (see the specific SW dimensions in the figure legend) characterized by an unbinding critical fugacity $k_{D_2,c} = 2.607536\ldots$ (exact calculation). Curves in panel (a) show, as k decreases, the following free energy profile evolution: i) a unique free energy minimum at $z = 0$

(for $k = 2.6100 > k_{D_2,c}$) which delocalizes into a wide one at $k = 2.6075 \simeq k_{D_2,c}^{(RSOS)}$ (i.e. the continuous transition in the pure wedges); ii) double minima profiles for $k = 2.6050, 2.6025 \lesssim k_{D_2,c}$ with the minima placed at $z = d_1 - d$ and $z = d_1$ (i.e. coexistence between the state localized at the SW central ridge height and the bulk unbound state); iii) dominance of bulk unbound state ($k = 2.6000 < k_{D_2,c}$). An analogous evolution is extracted by the free energy profiles of Δf_0 in panel (b). Therefore, in passing between ii) and iii) we have a discontinuous transition! Finally, the picture clarifies that the discontinuous nature of such transition is strictly related to the fact that, for diverging system size, d parameter maintains larger than the widths of the two free energy minima (scaling as $\sim W^{1/2}$).
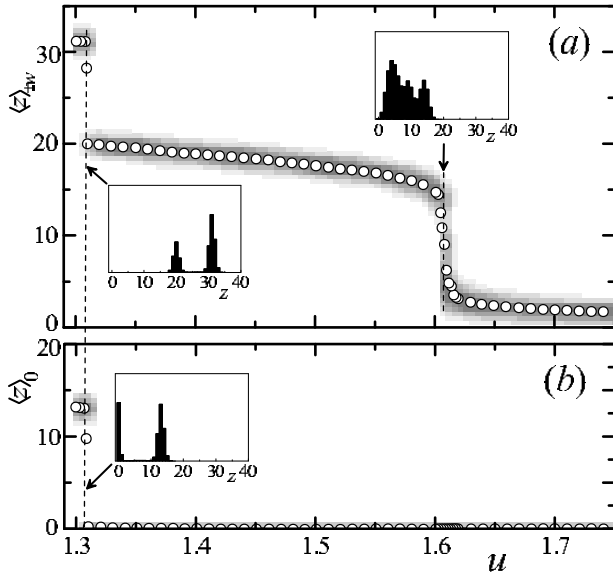

FIG. 5. Average interface distances (open dots) from $3D$ SW bottoms (panel (a)) and central ridge (panel (b)) and the corresponding distributions (gray shaded area). The data come from Metropolis Monte Carlo simulations at constant $t = 2.0$ and system sizes $L = 100$, $W = 50$, wall unit slope and $d_1/d = 2$ (i.e. $d = 16$). In the insets is the detail of interface distance distributions at the u values marked by the dashed lines.

IV. 3D STRUCTURED WEDGES

Transfer matrix approach is not applicable to the wetting problem in $3D$. In this case we have considered Metropolis Monte Carlo simulations of an RSOS fluctuating interface (see Fig. 2(b)) in a $3D$ SW geometry like the one sketched in Fig. 1(b). Because of rapid increase of computation times with system size, we have considered relatively small systems: the simulations were done for squared system with size $L = 50, 100, 150$ (in the y axis direction) and $W = L/2$ (L and W are in lattice units) and using periodic boundary conditions along both x

and y axes. The SWs considered in the simulations were usually constructed by (staircase) tilted walls with slope 1 or 1/2 and $d_1/d \simeq 2$ (see Fig. 1(b)). As usual, the implemented Metropolis Monte Carlo algorithm was based on local moves corresponding to the attempt of changing (at random) the local surface height by one unit (i.e. $z_{x,y} \to z_{x,y} \pm 1$). After equilibration, the calculation of equilibrium average parameters has been performed on the basis of very long simulations of up to $10^5 \div 10^6$ MCS (1 $MCS \equiv L^2$ Monte Carlo moves).

In Fig. 5, as a representative of the general behavior, we show the u dependence of the interface averages distances from SW bottoms ($\langle z \rangle_{\pm w}$, panel ($a$)) and SW central ridge ($\langle z \rangle_0$, panel (b)) obtained a constant t for a given $3D$ SW (see geometrical specifications in figure legend). The behavior of these two quantities follows a scheme very similar to the one outlined for $2D$ SW interface unbinding: i) a continuous filling–like transition of the two component wedges at $u \simeq 1.607$ (note also in the right inset in panel (a) the roughly flat height distribution); ii) a discontinuous detachment from the SW central ridge at $u \simeq 1.309$ (see the double peak structure of the interface height distributions in the left insets in panel (a) and (b)). However, at least for the finite size system considered here, continuous and discontinuous unbinding seem to be separated by a finite u gap. Most probably this is due to the linear extension of the system along y axis which corresponds to the main difference between the present $3D$ SW geometry and the $2D$ one. With an extensive simulations program, we planned to evaluate the whole interface phase–lines for $3D$ wedges with the intent to clarify also this aspect.

V. CONCLUSIONS

Our investigation demonstrate that interface unbinding in SWs takes place in two stages: the first one corresponds to the continuous filling transition of the two component wedges; in the second stage the interface jumps, discontinuously, from a state localized at the SW central ridge and the bulk unbound state. We stress the fact that in SWs the bulk unbound state come into field, rather than in some artificial way [17], just because of the *corrugated* geometry of the substrate. First–order nature of the final unbinding transition is due to the *competition* between binding at the central ridge and whole SW filling. In other words, it is the spatial combination of wedges and ridges of SWs to create the conditions for a discontinuous interface unbinding. As seen in section III, a single ridge is only able to strongly pin the interface retarding (with respect to a wedge) its unbinding from the apex (for more details see also ref. [15]). In complete wetting regime, as shown in ref. [13], interface unbinding near the apex mimics planar critical wetting.

Generalization of our conclusions to more complex SWs and/or to random rough surfaces should take into account, carefully, the type and the scaling properties of

the corrugation introduced by the specific boundary. On the other hand, our analysis about interface unbinding in $2D$ SWs give some more efforts on the key role of surface roughening exponent ζ_S in determining the nature of the wetting transition in self–affine rough substrates. In the light of the present results, we have started new investigations of $2D$ and $3D$ rough geometries, with the purpose to get conclusive insights in this issues.

[1] S. Dietrich, in *Phase Transition and Critical Phenomena*, edited by C. Domb and J. L. Lebowitz (Academic Press, London, 1988), vol. 12, p. 1.

[2] G. Forgacs, R. Lipowsky, and T. M. Nieuwenhuizen, in *Phase Transition and Critical Phenomena*, edited by C. Domb and J. L. Lebowitz (Academic Press, London, 1991), vol. 14, p. 135.

[3] P. Pfeifer, Y. J. Wu, M. W. Cole, and J. Krim, Phys. Rev. Lett. **62**, 1997 (1989).

[4] M. Kardar and J. O. Indekeu, Europhys. Lett. **12**, 161 (1990).

[5] A. O. Parry, A. J. Wood, and C. Rascòn, J. Phys.: Condens. Matter **12**, 7671 (2000).

[6] C. Rascòn and A. O. Parry, Nature **207**, 986 (2000).

[7] L. Bruschi, E. Carlin, and G. Mistura, J. Phys.: Condens. Matter **15**, S315 (2003).

[8] A. O. Parry, C. Rascon, and A. J. Wood, Phys. Rev. Lett. **83**, 5535 (1999).

[9] G. Giugliarelli and A. L. Stella, Phys. Rev. E **53**, 5035 (1996).

[10] G. Giugliarelli and A. L. Stella, Physica A **239**, 467 (1997).

[11] A. L. Stella and G. Sartoni, Phys. Rev. E **58**, 2979 (1998).

[12] G. Giugliarelli and A. L. Stella, J. Phys.: Math. Gen. **32**, 5409 (1999).

[13] A. O. Parry, M. J. Greenall, and J. M. Romero-Enrique, Phys. Rev. Lett. **90**, 046101 (2003).

[14] A. O. Parry, M. J. Greenall, and A. J. Wood, J. Phys.: Condens. Matter. **14**, 1169 (2002).

[15] G. Giugliarelli, submitted for publication.

[16] D. B. Abraham, Phys. Rev. Lett. **44**, 1165 (1980).

[17] Th. M. Nieuwenhuizen, J. Phys. A **21**, L567 (1988).